Optimal quantum superresolution for full distance between incoherent optical sources in two dimensions

Junyan Li¹ and Shengshi Pang^{1,2} * ¹ School of Physics, Sun Yat-sen University, Guangzhou, Guangdong 510275, China ² Hefei National Laboratory, University of Science and Technology of China, Hefei 230088, China

The Rayleigh criterion has long served as a fundamental limit for the resolution of optical imaging. Recent advances in multiparameter quantum metrology have led to quantum superresolution that can break this limit and achieve nonvanishing precision in estimating the separation between a pair of closely located incoherent point sources. For two-dimensional optical systems, the quantum superresolution has been studied for the Cartesian components of separation between two incoherent point sources. However, the precision limit of estimating the full distance between two point sources remains unknown so far. In this paper, we investigate the estimation precision of the full distance between two incoherent point sources with arbitrary intensities in a two-dimensional imaging system. Through the multiparameter quantum estimation theory, we obtain the ultimate estimation precision for the distance and show that it remains nonzero when the distance approaches zero, which surpasses the Rayleigh criterion. We further show the dependence of the estimation precision on the relative orientation between the two point sources, which leads to a novel scheme that can enhance the precision by aligning the sources along proper directions if the point-spread functions are not circularly symmetric, and the enhancement is determined by the extent to which the pointspread functions deviate from circular symmetry. Finally, the results are illustrated by incoherent sources with Gaussian point-spread functions.

I. INTRODUCTION

In recent years, quantum metrology has been rapidly advanced across a range of fields, including gravitational wave detection [1, 2], quantum clocks [2–5], quantum sensing [6, 7], quantum imaging [8–10] and provided new perspectives for the quantum-enhanced technologies that can boost the performance of measurements beyond the precision limit of their classical counterparts.

A notable example is the longstanding challenge of resolving closely spaced optical sources, which is constrained by Rayleigh criterion in classical optics [11]. This criterion sets a diffraction-limited resolution threshold at $d = 1.22\lambda/(2NA)$, with λ the wavelength of the light and NA the numerical aperture of the imaging system. To overcome this limit, various approaches have been proposed. One straightforward method is to reduce the wavelength or increase the numerical aperture [12]. More fundamentally, techniques such as microscopy structured illumination [13, 14], photoactivatable localization [15] and stochastic optical reconstruction microscopy [16] have been proposed to surpass the Rayleigh limit by exploiting nonlinear optical responses, stochastic activation of fluorescent emitters, and computational reconstruction algorithms. While these techniques have achieved remarkable progress in imaging resolution, they typically require specialized fluorophores, sophisticated control of activation cycles, or complex image processing

From a statistical perspective, when two incoherent optical sources have significant overlap on the image plane,

the precision of estimating their separation is fundamentally limited by the Cramér-Rao lower bound [18, 19]. It follows that the estimation precision of the separation between two optical sources vanishes as the separation approaches zero by direct imaging. This statistical phenomenon is known as Rayleigh's curse. However, Tsang et al. [20] attacked this problem from the perspective of quantum multiparameter estimation and surprisingly found that the quantum Cramér-Rao bound (QCRB) [21] does not vanish for arbitrarily small separation of two incoherent point sources if the quantum measurements on the point sources are optimized, which addresses Rayleigh's curse.

Since Tsang et al.'s breakthrough, the quantum superresolution has been verified experimentally by various techniques, e.g., image inversion interferometry [22], heterodyne detection [23], edge coherence inversion [24], two-photon interference [25, 26], and digital holography [27]. In parallel, theoretical advances have obtained the optimal observables and estimators for the quantum superresolution [28, 29] and extended the quantum superresolution framework to thermal states [30], detector noise [31, 32], dark states [33], arbitrary source distributions [34, 35], moment estimation [36–38]. Further developments have considered the influence of unknown intensities of the optical sources which leads to the resurgence of Rayleigh's curse [39], and studied the roles of coherence [40–44] and partial coherence [45–49] of optical sources in preventing the resurgence of Rayleigh's curse. The feasibility conditions of superresolution given unknown intensities of the point sources have also been obtained [50]. These efforts have also enabled the application of quantum superresolution in source localization [51, 52], time-frequency resolution [53–57], etc.

In the original superresolution protocol [20], the su-

^{*} pangshsh@mail.sysu.edu.cn

perresolution was proposed for two optical sources with one-dimensional point-spread functions. However, the point-spread functions of practical optical sources are essentially multidimensional, where the spatial structures of the point-spread functions become crucial to the imaging resolution. In this broader context, multiparameter quantum estimation theory provides a powerful tool to improve the imaging precision [58–61]. Building upon this foundation, subsequent researches have extended the quantum superresolution to the estimation of Cartesian components of the separation for two-dimensional point sources [62] and for three-dimensional point sources [63– 65], and to more complex imaging tasks such as surface metrology [66], using balanced homodyne detection [67], and estimating the sizes of uniform line and disk sources [68], etc.

In this work, we investigate the quantum precision limits of two-dimensional superresolution for a pair of incoherent point sources with arbitrary relative intensities. Rather than the individual Cartesian components of the separation, we focus on the quantum estimation of the full distance between two point sources. We show that, by optimizing the measurement basis, the quantum Fisher information for the distance remains finite when the two sources get close to each other, which breaks the Rayleigh limit. Furthermore, when the point-spread functions (PSF) of the two point sources are not circularly symmetric, the estimation precision exhibits a nontrivial dependence on the relative orientation between the two point sources. This orientation dependence enables further precision enhancement by aligning the two point sources along specific directions. We optimize the quantum Fisher information of the distance over the azimuth between the two point sources, and obtain the optimal azimuth and the maximum quantum Fisher information for the estimation of source distance. Taking Gaussian PSFs as an example, we find that the optimal orientation corresponds to the minor axis of the PSF.

II. PRELIMINARIES

A. Model of optical sources

For a spatially invariant imaging system, suppose two incoherent optical pointlike sources are located at unknown positions (X_1, Y_1) and (X_2, Y_2) on the object plane, and separated by a distance r. In the Poisson limit, the probability of multiple photons arriving at the imaging plane simultaneously is negligible [59], within a given coherence time interval. The average state of a single photon that arrived at the imaging plane can be described by a density operator [69],

$$\hat{\rho} = \frac{1 - \epsilon}{2} |\psi_1\rangle\langle\psi_1| + \frac{1 + \epsilon}{2} |\psi_2\rangle\langle\psi_2|,\tag{1}$$

where ϵ is the intensity imbalance parameter

$$\epsilon = \frac{N_2 - N_1}{N_2 + N_1},\tag{2}$$

and N_1 and N_2 are the average photon numbers emitted by the two point sources respectively. $|\psi_{1,2}\rangle$ are the spatially shifted states from a fixed state $|\psi\rangle$, given by

$$|\psi_{1,2}\rangle = \exp(-iY_{1,2}\hat{P}_y - iX_{1,2}\hat{P}_x)|\psi\rangle,$$
 (3)

where $\hat{P}_k = -i\partial_k$, k = x, y, are the momentum operators in the x, y directions respectively, and the state $|\psi\rangle$ is

$$|\psi\rangle = \int_{-\infty}^{\infty} dy \int_{-\infty}^{\infty} dx \psi(x, y) |x, y\rangle,$$
 (4)

where $\psi(x,y)$ is the point-spread function of the imaging system, assumed to be real and inversion-symmetric throughout this work, i.e., $\psi(x,y) = \psi(-x,-y)$.

For two-dimensional imaging systems, in addition to the distance between two point sources, the relative orientation also play a critical role in the imaging resolution, so we will focus on both the distance and the azimuth between two point sources in this work. To this end, we define the distance between two point sources as r and the azimuth between the sources, i.e., the angle between the displacement of the sources and a fixed reference axis, as $\alpha \in [0, \pi]$, which is illustrated in Fig. 1. The positions of the two sources can then be written as

$$(X_{1,2}, Y_{1,2}) = \left(\bar{X} \mp \frac{r}{2} \cos\alpha, \bar{Y} \mp \frac{r}{2} \sin\alpha\right), \qquad (5)$$

where the subscript 1,2 and the \mp sign denote the two sources respectively, and the centroid vector (\bar{X}, \bar{Y}) is defined as

$$(\bar{X}, \bar{Y}) = (\frac{X_2 + X_1}{2}, \frac{Y_2 + Y_1}{2}).$$
 (6)

The displacement between the two point sources can be denoted as

$$(d_x, d_y) = (X_2 - X_1, Y_2 - Y_1). (7)$$

In this case, the momentum operator along the displacement between the two sources can be defined as

$$\hat{P}_r = \hat{P}_x \cos \alpha + \hat{P}_y \sin \alpha, \tag{8}$$

with its orthogonal complement given by

$$\hat{P}_{r^{\perp}} = -\hat{P}_x \sin \alpha + \hat{P}_y \cos \alpha. \tag{9}$$

It is worth noting that while the azimuth α is defined with respect to a specific reference axis, it characterizes the *relative* orientation between the two point sources which is intrinsic to the two point sources. This is manifested by the fact that the overlap between the two point sources,

$$\delta = \langle \psi_1 | \psi_2 \rangle = \langle \cos(r\hat{P}_r) \rangle, \tag{10}$$

is dependent on the azimuth α with respect to a given axis, as illustrated in Fig. 2. So, even though the azimuth α can change with the reference axis, the relative orientation it defines as well as the impact of the relative orientation on the resolution of the two point sources does not change. This will be clearer when we obtain the quantum Fisher information for the distance later.

As shown in Fig. 2, the overlap between the point-spread functions of the two optical sources leads to the non-orthogonality of their associated quantum states, which in turn constrains the distinguishability between them. In particular, when the distance is comparable to or even smaller than the width of the point-spread function, the two point sources becomes essentially indistinguishable, which is known as Rayleigh's curse. This raises a challenging question: how can one estimate the distance between two incoherent point sources, particularly when the distance goes to zero?

This question has been addressed for one-dimensional imaging systems by the pioneering work of Tsang et al., and also been considered for the estimation of the orthogonal components of the separation between two point sources in two-dimensional imaging systems, as reviewed in the introduction section. In this work, we will focus on the estimation of the full distance, as well as the relative orientation, between two point sources in two-dimensional imaging systems.

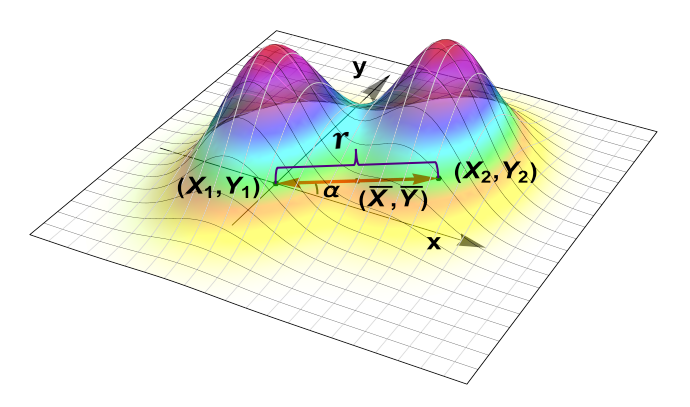


Figure 1: Two point optical sources located at (X_1, Y_1) and (X_2, Y_2) . The distance between the two sources is r, and the *relative* orientation between the two point sources characterized by the azimuth α , i.e., the angle between the displacement of the two sources and a given reference axis which is the x axis in the figure.

B. Precision limit of direct imaging

The most straightforward measurement scheme to resolve two closely located point sources is the direct imaging, wherein the information about the positions of the point sources can be extracted from the intensity distribution of the photons arriving at the image plane.

Suppose the photon counting at a small area $dx \times dy$

around the position (x, y) of the image plane is approximately $(N_1 + N_2)p_{\mathbf{g}}(x, y)$ dxdy, where $p_{\mathbf{g}}(x, y)$ is the position distribution of a single photon arriving on the image plane,

$$p_{\mathbf{g}}(x,y) = \frac{1-\epsilon}{2} \Lambda(x - X_1, y - Y_1) + \frac{1+\epsilon}{2} \Lambda(x - X_2, y - Y_2), \tag{11}$$

and it depends on four parameters collected in the vector \mathbf{g} : the distance r, the azimuth α and the centroid positions (\bar{X}, \bar{Y}) , i.e.,

$$\mathbf{g} = (\bar{X}, \bar{Y}, r, \alpha)^{\top}. \tag{12}$$

The intensity $\Lambda(x, y)$ is determined by the point-spread function $\psi(x, y)$ of the imaging system,

$$\Lambda(x,y) = |\psi(x,y)|^2. \tag{13}$$

To resolve two optical point sources, it is essential to measure and estimate the parameter vector **g**.

For any unbiased estimator $\hat{\mathbf{g}} = (\widehat{X}, \widehat{Y}, \widehat{r}, \widehat{\alpha})^{\mathsf{T}}$, the covariance matrix of the estimation is lower bounded by the well-known Cramér-Rao inequality [21, 70, 71],

$$Cov[\hat{\mathbf{g}}] \ge N_{\text{tot}}^{-1} \mathcal{J}^{-1}[\mathbf{g}], \tag{14}$$

where N_{tot} is total number of photons from the two optical sources,

$$N_{\text{tot}} = N_1 + N_2. (15)$$

The " \geq " sign represents semi-definite positivity of matrix, and $\mathcal{J}[\mathbf{g}]$ is the Fisher information matrix per detected photon. When the photon numbers N_{tot} are sufficiently large, the Cramér-Rao bound inequality can always be asymptotically achieved [21].

For a small distance r, the estimation precision using the direct imaging method is given by

$$\mathcal{H}_r^{\text{(direct)}} = N_{\text{tot}}/(\mathcal{J}^{-1})_{33} = \frac{r^2 \left(1 - \epsilon^2\right)^2 N_{\text{tot}}}{32} \mathcal{A}, \quad (16)$$

as derived in Appendix A, where \mathcal{A} is independent of the distance r. This result implies that, by direct imaging, the estimation precision $\mathcal{H}_r^{(\mathrm{direct})}$ decays quadratically with r and thus vanishes in the limit $r \to 0$. This phenomenon is called Rayleigh's curse [20].

III. SUPERRESOLUTION FOR TWO-DIMENSIONAL POINT SOURCES

A. Quantum precision limit for separation of point sources

Although direct imaging is a standard imaging method which is straightforward to implement, it is only one of the possible measurement methods allowed by quantum mechanics.

For the current quantum superresolution problem, the quantum state of a single photon is described by the density operator $\hat{\rho}$ (1), which depends on a set of unknown parameters $\mathbf{g} = (\bar{X}, \bar{Y}, r, \alpha)^{\top}$ (12). A brief review of quantum estimation theory in the context of this problem is provided in Appendix B1, where it is shown that the estimation precision of the parameter vector \mathbf{g} is fundamentally constrained by the quantum Cramér–Rao bound (QCRB),

$$Cov[\hat{\mathbf{g}}] \ge N_{\text{tot}}^{-1} \mathcal{Q}_{ij}^{-1}[\mathbf{g}], \tag{17}$$

where Q is the quantum Fisher information matrix, determined by the quantum state $\hat{\rho}$ to be measured.

In fact, the quantum Cramér-Rao bound for multiparameter estimation is not always achievable due to the potential non-commutativity between the optimal measurements for different parameters. But one can introduce a positive-semidefinite weight matrix W to assign different weights with different parameters, yielding a scalar bound

$$\operatorname{Tr}(WC) \ge N_{\operatorname{tot}}^{-1} \operatorname{Tr}(WQ^{-1}).$$
 (18)

This scalar bound is saturable when

$$\operatorname{Tr}(\hat{\rho}[\hat{\mathcal{L}}_{g_i}, \hat{\mathcal{L}}_{g_i}]) = \operatorname{Im}\operatorname{Tr}(\hat{\rho}\hat{\mathcal{L}}_{g_i}\hat{\mathcal{L}}_{g_i}) = 0, \tag{19}$$

where $\hat{\mathcal{L}}_{g_i}$ denotes the symmetric logarithmic derivative (SLD) with respect to parameter g_i , since the quantum Cramér-Rao bound coincides with the Holevo bound when this condition holds and the latter is always asymptotically achievable with a sufficiently large number of states [39, 58]. In our model, this condition is fulfilled due to the reality of $\psi(x)$, which makes the symmetric logarithmic derivatives $\hat{\mathcal{L}}_{g_i}$ and $\hat{\mathcal{L}}_{g_j}$ also real and hence $\text{Tr}(\hat{\rho}\hat{\mathcal{L}}_{g_i}\hat{\mathcal{L}}_{g_j})$ real as well. Therefore, the quantum Cramér-Rao bound provides an achievable precision limit to quantum superresolution.

By diagonalizing $\hat{\rho}$, the quantum Fisher information matrix with respect to the four unknown parameters $\bar{X}, \bar{Y}, r, \alpha$ can be obtained straightforwardly by its definition. As the derivation and the result are lengthy, they are provided in Appendix B 2.

In the limit $r \to 0$, the precision \mathcal{H}_r is simplified to

$$\mathcal{H}_r|_{r\to 0} = \frac{N_{\text{tot}} \left(1 - \epsilon^2\right) \left(\kappa_x \kappa_y - \eta^2\right)}{\kappa_{r^{\perp}}}, \qquad (20)$$

where

$$\eta = \langle \hat{P}_x \hat{P}_y \rangle, \; \kappa_i = \langle \hat{P}_i^2 \rangle, i = x, y, r^{\perp}, \eqno(21)$$

and r^{\perp} is the direction orthogonal to r. This result demonstrates that, while direct imaging fails with vanishing precision in the sub-Rayleigh regime, an optimized quantum measurement scheme can achieve non-vanishing precision, thus beating Rayleigh's curse.

Notably, as aforementioned, the azimuth α between the two point sources is defined with respect to a specific

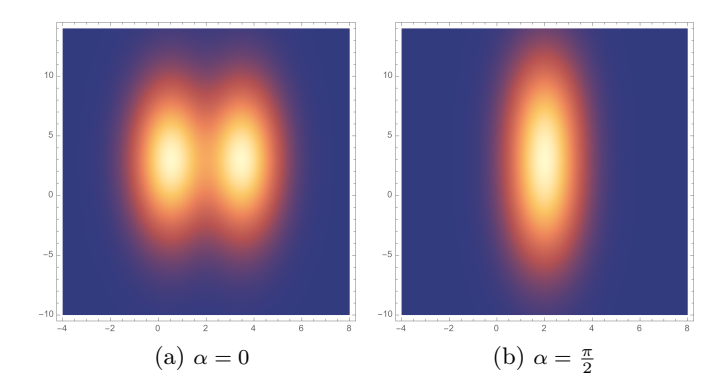


Figure 2: The probability distribution p(x,y) for detecting a single photon from two point sources with identical Gaussian point-spread functions on a two-dimensional image plane with respect to the different azimuth α . The plots show how the spatial overlap δ between the two point-spread functions and the probability distribution of photon detection varies with the azimuth α .

reference axis, which can be changed with the coordinating system, but the relative orientation between the two point sources is inherent to the two sources and the impact of the relative orientation on the superresolution precision is independent of the choice of coordinate system. This is particularly manifested by the result \mathcal{H}_r . While \mathcal{H}_r is dependent on the azimuth α , the precision \mathcal{H}_r turns out to be invariant with any rotation of the coordinate system. A detailed proof for this coordinate invariance of \mathcal{H}_r is provided in Appendix B 3.

It can be immediately seen from Eq. (20) that the estimation precision \mathcal{H}_r attains its maximum over ϵ when the intensities of two optical sources are balanced, i.e., $\epsilon = 0$. In this case, the precision \mathcal{H}_r (20) can be further simplified to

$$\mathcal{H}_r|_{r\to 0} = \frac{N_{\text{tot}}\left(\kappa_x \kappa_y - \eta^2\right)}{\kappa_{r\perp}}.$$
 (22)

Any deviation from this balance leads to a degradation in precision. Counterintuitively, this suggests that introducing asymmetry to the intensities of two sources, while increasing the visual contrast of the intensity distribution on the image plane, actually reduces the resolvability of the two sources. Physically, this is because the resolution of two optical sources relies on the distinguishability between them and lowering the intensity of either source will decrease its distinguishability from the other. For example, if the intensity of one source is tuned to zero, the visual contrast on the image plane reaches the maximum, but that source can never be distinguished from the other as it is impossible to determine its location when its intensity is zero.

B. Optimization for precision limit of distance

As explicitly seen from Eq. (20), the estimation precision \mathcal{H}_r depends sensitively on the azimuth α , leading to an interesting question: Can the precision \mathcal{H}_r be enhanced through properly aligning the two sources?

We derive the optimal azimuth and the highest precision by solving

$$\partial \mathcal{H}_r|_{r\to 0} / \partial \alpha = 0, \tag{23}$$

where $\mathcal{H}_r|_{r\to 0}$ is given in Eq. (20). The optimal and the worst azimuths can worked out as

$$\alpha_{\text{opt/wor}} = \tan^{-1} \left(\frac{\kappa_y - \kappa_x \pm \sqrt{4\eta^2 + (\kappa_y - \kappa_x)^2}}{2\eta} \right),$$
(24)

and the corresponding highest and lowest precision in the limit $r \to 0$ reads

$$\left. \mathcal{H}_r^{(\text{opt/wor})} \right|_{r \to 0} = \frac{N_{\text{tot}} \left(1 - \epsilon^2 \right)}{2} \times \left(\kappa_x + \kappa_y \pm \sqrt{4\eta^2 + (\kappa_y - \kappa_x)^2} \right). \tag{25}$$

The precision enhancement of properly aligning the two point sources can be characterized by the ratio

$$\xi = \frac{\mathcal{H}_r^{(\alpha_{\text{opt}})}}{\mathcal{H}_r^{(\alpha_{\text{wor}})}} = \frac{\kappa_x + \kappa_y + \sqrt{4\eta^2 + (\kappa_y - \kappa_x)^2}}{\kappa_x + \kappa_y - \sqrt{4\eta^2 + (\kappa_y - \kappa_x)^2}}.$$
 (26)

Whenever the point-spread function is not circularly symmetric, $\kappa_y \neq \kappa_x$ and $\sqrt{4\eta^2 + (\kappa_y - \kappa_x)^2} > 0$, hence it indicates that optimal alignment of the two point sources can enhances the superresolution precision significantly.

In particular, when the point-spread function of the imaging system has reflection symmetry, e.g., $\psi(x,y) = \psi(x,-y) = \psi(-x,-y)$, the term $\eta = \langle \hat{P}_x \hat{P}_y \rangle$ vanishes [62], and the estimation precision \mathcal{H}_r (20) is simplified to

$$\mathcal{H}_r|_{r\to 0} = \frac{N_{\rm tot}\kappa_x\kappa_y}{\sin^2\alpha\kappa_x + \cos^2\alpha\kappa_y},\tag{27}$$

with the optimal azimuth as

$$\alpha_{\text{opt}} = \begin{cases} 0, & \text{if } \kappa_x > \kappa_y, \\ \frac{\pi}{2}, & \text{if } \kappa_x < \kappa_y, \end{cases}$$
 (28)

and the worst azimuth as

$$\alpha_{\text{wor}} = \alpha_{\text{opt}} + \frac{\pi}{2}.$$
 (29)

In this scenario, the highest and the lowest precision reads

$$\mathcal{H}_r^{(\text{opt/wor})} = (1 - \epsilon^2) N_{\text{tot}} \kappa_{\text{max/min}},$$
 (30)

where κ_{\max} and κ_{\min} are the maximum and the minimum of κ_x and κ_y respectively, and the ratio ξ between the highest and the lowest precisions becomes

$$\xi = \frac{\kappa_{\text{max}}}{\kappa_{\text{min}}},\tag{31}$$

implying that the more the point-spread function deviates from the circular symmetry, the higher the superresolution precision can be increased by proper aligning of the two point sources.

C. Example: two-dimensional Gaussian point-spread functions

To illustrate above results, we consider a typical Gaussian point-spread functions for the imaging system,

$$\psi_i(x,y) = \frac{\exp\left[-\frac{1}{4} (f - \mu_i)^\top \Sigma^{-1} (f - \mu_i)\right]}{(2\pi)^{1/2} |\Sigma|^{1/4}}, \ i = 1, 2,$$
(32)

where $f = (x, y)^{\top}$ is the spatial coordinate vector, and $\mu_i = (X_i, Y_i)^{\top}$ denotes the position of the *i*-th source. The covariance matrix Σ is defined as

$$\Sigma = \begin{pmatrix} \sigma_1^2 & \beta \sigma_1 \sigma_2 \\ \beta \sigma_2 \sigma_1 & \sigma_2^2 \end{pmatrix}, \tag{33}$$

where σ_1 and σ_2 are the widths of the Gaussian distribution along the x and y axis respectively, and $\beta \in [-1, 1]$ quantifies the correlation.

The spatial characteristics of a Gaussian point-spread function is fully captured by its covariance matrix Σ (33), whose eigenvectors determine the orientations of the major and minor axes,

$$\Phi_{\pm} = \tan^{-1} \frac{\sigma_2^2 - \sigma_1^2 \pm \Re}{2\beta \sigma_1 \sigma_2},\tag{34}$$

where $\Re \equiv \sqrt{(\sigma_2^2 - \sigma_1^2)^2 + 4\beta^2 \sigma_2^2 \sigma_1^2}$, and Φ_{\pm} are the angles of the major and minor axes with respect to the horizontal axis, respectively. Additionally, the quantities in Eq. (20) become

$$\kappa_x = \frac{1}{4\sigma_1^2 (1 - \beta^2)},$$

$$\kappa_y = \frac{1}{4\sigma_2^2 (1 - \beta^2)},$$

$$\eta = -\frac{\beta}{4\sigma_1\sigma_2 (1 - \beta^2)}.$$
(35)

For two Gaussian point sources with arbitrary intensities, the estimation precision of the distance r in the limit $r \to 0$ is

$$\mathcal{H}_r|_{r\to 0} = \frac{N_{\text{tot}} \left(1 - \epsilon^2\right)}{4 \left(\beta \sigma_2 \sigma_1 \sin(2\alpha) + \sigma_1^2 \cos^2 \alpha + \sigma_2^2 \sin^2 \alpha\right)},\tag{36}$$

it can be seen that the estimation precision \mathcal{H}_r remains nonzero in the sub-Rayleigh limit and shows its dependence on the azimuth α .

The extrema of the precision \mathcal{H}_r over the azimuth α can be determined by the stationary condition

$$\partial \mathcal{H}_r / \partial \alpha = 0, \tag{37}$$

which gives the optimal and the worst α as

$$\alpha_{\text{opt/wor}} = \tan^{-1} \frac{\sigma_2^2 - \sigma_1^2 \mp \Re}{2\beta \sigma_1 \sigma_2}.$$
 (38)

One can observe that $\alpha_{\rm opt}=\Phi_{-}$ and $\alpha_{\rm wor}=\Phi_{+}$, implying that the extrema of the estimation precision \mathcal{H}_{r} occurs when the displacement between the two point sources aligns with one of the principal axes of the Gaussian point-spread function. The optimal and the worst precision \mathcal{H}_{r} as $r\to 0$ are given by

$$\left. \mathcal{H}_r^{(\alpha_{\text{opt/wor}})} \right|_{r \to 0} = \frac{N_{\text{tot}} \left(1 - \epsilon^2 \right) \left(\sigma_1^2 + \sigma_2^2 \pm \Re \right)}{8 \left(1 - \beta^2 \right) \sigma_1^2 \sigma_2^2}, \quad (39)$$

which indicates that the optimal estimation precision \mathcal{H}_r is achieved when the displacement between the two point sources aligns with the minor axis of the Gaussian point-spread function.

The enhancement ratio ξ by optimizing the aligning of the two point sources in this case is given by

$$\xi = \frac{\sigma_1^2 + \sigma_2^2 + \Re}{\sigma_1^2 + \sigma_2^2 - \Re}.$$
 (40)

The above results can be further simplified for a Gaussian point-spread function with reflection symmetry about the x and y axes, i.e., $\beta=0$ and $\Phi_+=0$, $\Phi_-=\frac{\pi}{2}$. In this case, the estimation precision \mathcal{H}_r (36) becomes

$$\mathcal{H}_r|_{r\to 0} = \frac{\left(1 - \epsilon^2\right) N_{\text{tot}}}{4\left(\sigma_2^2 \sin^2 \alpha + \sigma_1^2 \cos^2 \alpha\right)}.\tag{41}$$

The optimal azimuth α for \mathcal{H}_r is

$$\alpha_{\text{opt}} = \begin{cases} \frac{\pi}{2}, & \text{if } w < \sigma, \\ 0, & \text{if } \sigma < w, \end{cases}$$
 (42)

and the highest precision turns out to be

$$\max \mathcal{H}_r|_{r\to 0} = \frac{\left(1 - \epsilon^2\right) N_{\text{tot}}}{4\sigma_{\min}^2}.$$
 (43)

Similarly, the worst azimuth is

$$\alpha_{\rm wor} = \alpha_{\rm opt} + \frac{\pi}{2},$$
(44)

and the lowest precision is

$$\min \mathcal{H}_r|_{r\to 0} = \frac{\left(1 - \epsilon^2\right) N_{\text{tot}}}{4\sigma_{\text{max}}^2}.$$
 (45)

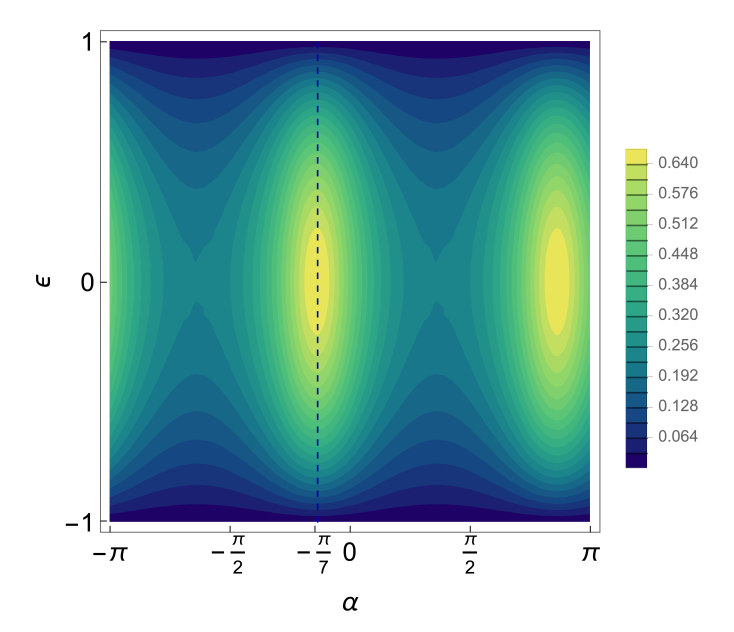


Figure 3: Density plot of the distance precision \mathcal{H}_r for two Gaussian point-spread functions with respect to the azimuth α and and the ratio ϵ of the photon number difference to the total photon number as $r \to 0$. $\sigma_1 = 1$, $\sigma_2 = 1.4$ and $\beta = 0.4$. It can be observed that when the azimuth α is fixed, the estimation precision of the distance r will decrease as the ratio ϵ increases and the optimal estimation precision can be always reached when the photon numbers of the two sources are the same, i.e., $\epsilon = 0$, showing the negative impact of photon number difference on the superresolution precision. On the other hand, when ϵ is fixed, the estimation precision of the distance varies with the azimuth α , and the maximum precision of the distance r can be obtained when α is approximately $-\pi/7$, which corresponds to the direction along the minor axis of the Gaussian point-spread function, implying the precision of estimating the distance can be enhanced by optimizing the relative orientation between the two point sources.

These results confirm that the maximum estimation precision is attained when the two point sources are aligned along the minor axis of the Gaussian point-spread function, in accordance with the general analysis above. The maximum enhancement by the alignment of the point sources is therefore

$$\xi = \frac{\sigma_{\text{max}}^2}{\sigma_{\text{min}}^2},\tag{46}$$

which implies that it is always possible to increase the superresolution precision by aligning the two point sources whenever the Gaussian point-spread function is not circularly symmetric. On the other hand, when the Gaussian point-spread function has circular symmetry, the overlap between the two point-spread functions always remains the same regardless of the aligning of the two sources, so in this case, the precision becomes orientation-

independent and there is no advantage in the precision by aligning the two sources.

To illustrate the above results numerically, Fig. 3 plots the estimation precision \mathcal{H}_r with respect to α and ϵ in the limit $r \to 0$. It can be seen that for a fixed azimuth α , the superresolution precision \mathcal{H}_r is maximized at $\epsilon = 0$, corresponding to the case of equal photon intensities. As ϵ increases, \mathcal{H}_r decreases and eventually vanishes with strong photon intensity imbalance. Moreover, for a given ϵ , \mathcal{H}_r shows clear dependence on the azimuth α between the two point sources, reaching its maximum at

$$\alpha_{\text{opt}} = \tan^{-1} \frac{\sigma_2^2 - \sigma_1^2 - \Re}{2\beta\sigma_1\sigma_2},\tag{47}$$

which coincides with the minor axis of the Gaussian point-spread function.

IV. CONCLUSION

In this work, we have explored the quantum limits of superresolution for two incoherent optical point sources in a two-dimensional imaging system with arbitrary intensity imbalance. By employing the multiparameter quantum estimation theory, we derived the ultimate precision bounds for estimating both the distance and the relative orientation (i.e., the azimuth) between the two sources. Our results demonstrate that, unlike classical direct imaging which suffers from Rayleigh's curse, quan-

tum strategies can yield nonzero precision even when the distance between the sources approaches zero. This confirms that the distance can be resolved beyond the classical diffraction limit through appropriate quantum measurements.

Moreover, we found that the superresolution precision for distance estimation has dependence on the relative orientation between two point sources, which led us to find that the estimation precision of distance can be significantly enhanced by aligning the two sources along specific directions and derive the optimal relative azimuth and the highest estimation precision of the distance between the two sources. This opens a new avenue for optimizing superresolution strategies in practical systems without circular symmetry.

In summary, our findings refine the current understanding of quantum superresolution and its ultimate capabilities in higher-dimensional imaging systems, offering both theoretical insight and practical guidance for the application of quantum superresolution in realistic scenarios.

ACKNOWLEDGMENTS

This work is supported by the National Natural Science Foundation of China (Grant No. 12075323), the Natural Science Foundation of Guangdong Province of China (Grant No. 2025A1515011440) and the Innovation Program for Quantum Science and Technology (Grant no. 2021ZD0300702).

- R. X. Adhikari, Reviews of Modern Physics 86, 121 (2014).
- [2] A. Roura, Physical Review X 10, 021014 (2020).
- [3] A. D. Ludlow, M. M. Boyd, J. Ye, E. Peik, and P. O. Schmidt, Reviews of Modern Physics 87, 637 (2015).
- [4] M. P. Woods, R. Silva, G. Pütz, S. Stupar, and R. Renner, PRX Quantum 3, 010319 (2022).
- [5] X.-B. Song, D.-Q. Xu, H.-B. Wang, J. Xiong, X. Zhang, D.-Z. Cao, and K. Wang, Applied Physics Letters 103, 131111 (2013).
- [6] C. L. Degen, F. Reinhard, and P. Cappellaro, Reviews of Modern Physics 89, 035002 (2017).
- [7] S. Pirandola, B. R. Bardhan, T. Gehring, C. Weedbrook, and S. Lloyd, Nature Photonics 12, 724 (2018).
- [8] G. B. Lemos, V. Borish, G. D. Cole, S. Ramelow, R. Lapkiewicz, and A. Zeilinger, Nature 512, 409 (2014).
- [9] P.-A. Moreau, E. Toninelli, T. Gregory, and M. J. Padgett, Nature Reviews Physics 1, 367 (2019).
- [10] C. A. Pérez-Delgado, M. E. Pearce, and P. Kok, Physical Review Letters 109, 123601 (2012).
- [11] Rayleigh, The London, Edinburgh, and Dublin Philosophical Magazine and Journal of Science 8, 261 (1879).
- [12] A. Schropp, R. Hoppe, J. Patommel, D. Samberg, F. Seiboth, S. Stephan, G. Wellenreuther, G. Falkenberg, and C. G. Schroer, Applied Physics Letters 100, 253112

(2012).

- [13] M. G. L. Gustafsson, Proceedings of the National Academy of Sciences 102, 13081 (2005).
- [14] E. Rittweger, K. Y. Han, S. E. Irvine, C. Eggeling, and S. W. Hell, Nature Photonics 3, 144 (2009).
- [15] E. Betzig, G. H. Patterson, R. Sougrat, O. W. Lind-wasser, S. Olenych, J. S. Bonifacino, M. W. Davidson, J. Lippincott-Schwartz, and H. F. Hess, Science 313, 1642 (2006).
- [16] M. J. Rust, M. Bates, and X. Zhuang, Nature Methods 3, 793 (2006).
- [17] S. Weisenburger and V. Sandoghdar, Contemporary Physics 56, 123 (2015).
- [18] S. M. Kay, Fundamentals of Statistical Signal Processing, Prentice Hall Signal Processing Series (Prentice-Hall PTR, Englewood Cliffs, N.J, 1993).
- [19] J. Zmuidzinas, Journal of the Optical Society of America A 20, 218 (2003).
- [20] M. Tsang, R. Nair, and X.-M. Lu, Physical Review X 6, 031033 (2016).
- [21] C. W. Helstrom, Journal of Statistical Physics 1, 231 (1969).
- [22] Z. S. Tang, K. Durak, and A. Ling, Optics Express 24, 22004 (2016).

- [23] F. Yang, A. Tashchilina, E. S. Moiseev, C. Simon, and A. I. Lvovsky, Optica 3, 1148 (2016).
- [24] W.-K. Tham, H. Ferretti, and A. M. Steinberg, Physical Review Letters 118, 070801 (2017).
- [25] M. Parniak, S. Borówka, K. Boroszko, W. Wasilewski, K. Banaszek, and R. Demkowicz-Dobrzański, Physical Review Letters 121, 250503 (2018).
- [26] J. A. Thachil, B. Ramanan, and A. Kumar, Physica Scripta 98, 115126 (2023).
- [27] M. Paúr, B. Stoklasa, Z. Hradil, L. L. Sánchez-Soto, and J. Rehacek, Optica 3, 1144 (2016).
- [28] G. Sorelli, M. Gessner, M. Walschaers, and N. Treps, Physical Review Letters 127, 123604 (2021).
- [29] G. Sorelli, M. Gessner, M. Walschaers, and N. Treps, Physical Review A 104, 033515 (2021).
- [30] R. Nair and M. Tsang, Physical Review Letters 117, 190801 (2016).
- [31] C. Lupo, Physical Review A 101, 022323 (2020).
- [32] M. Tsang, Physical Review A 107, 012611 (2023), arxiv:2209.06104 [quant-ph].
- [33] M. C. Brennan, M. Howard, Y. Marzouk, and L. E. Dresselhaus-Marais, Journal of Materials Science 57, 14890 (2022), arxiv:2203.05671 [cond-mat].
- [34] M. Tsang, Quantum 5, 527 (2021), arxiv:2103.08532 [physics, physics:quant-ph].
- [35] E. F. Matlin and L. J. Zipp, Scientific Reports 12, 2810 (2022).
- [36] X.-J. Tan, L. Qi, L. Chen, A. J. Danner, P. Kanchanawong, and M. Tsang, Optica 10, 1189 (2023).
- [37] M. Tsang, Physical Review A 99, 012305 (2019).
- [38] S. Zhou and L. Jiang, Physical Review A **99**, 013808 (2019).
- [39] J. Řehaček, Z. Hradil, B. Stoklasa, M. Paúr, J. Grover, A. Krzic, and L. L. Sánchez-Soto, Physical Review A 96, 062107 (2017).
- [40] Z. Hradil, J. Řeháček, L. Sánchez-Soto, and B.-G. Englert, Optica 6, 1437 (2019), arxiv:1910.10265 [physics, physics:quant-ph].
- [41] K. Liang, S. A. Wadood, and A. N. Vamivakas, Optica 8, 243 (2021).
- [42] A. M. Zheltikov, Journal of Raman Spectroscopy 53, 1094 (2022).
- [43] I. Karuseichyk, G. Sorelli, M. Walschaers, N. Treps, and M. Gessner, Physical Review Research 4, 043010 (2022).
- [44] K. Liang, S. A. Wadood, and A. N. Vamivakas, Physical Review A 104, 022220 (2021), arxiv:2105.06817 [physics].
- [45] W. Larson and B. E. A. Saleh, Optica 5, 1382 (2018).
- [46] M. Tsang and R. Nair, Optica 6, 400 (2019).
- [47] W. Larson and B. E. A. Saleh, Optica 6, 402 (2019).
- [48] S. A. Wadood, K. Liang, Y. Zhou, J. Yang, M. A. Alonso, X.-F. Qian, T. Malhotra, S. M. H. Rafsanjani, A. N. Jordan, R. W. Boyd, and A. N. Vamivakas, Optics Express 29, 22034 (2021), arxiv:2102.01603 [physics,

- physics:quant-ph].
- [49] K. Liang, S. A. Wadood, and A. N. Vamivakas, Optics Express 31, 2726 (2023).
- [50] J. Li and S. Pang, Physical Review A 110, 042620 (2024).
- [51] S. Prasad, Physical Review A 102, 033726 (2020).
- [52] E. Bisketzi, D. Branford, and A. Datta, New Journal of Physics 21, 123032 (2019).
- [53] B. Niewelt, M. Jastrzębski, S. Kurzyna, J. Nowosielski, W. Wasilewski, M. Mazelanik, and M. Parniak, Physical Review Letters 130, 240801 (2023).
- [54] V. Ansari, B. Brecht, J. Gil-Lopez, J. M. Donohue, J. Řeháček, Z. Hradil, L. L. Sánchez-Soto, and C. Silberhorn, PRX Quantum 2, 010301 (2021).
- [55] M. Mazelanik, A. Leszczyński, and M. Parniak, Nature Communications 13, 691 (2022).
- [56] C. S. Mitchell and M. P. Backlund, Physical Review A 105, 062603 (2022).
- [57] J. M. Donohue, V. Ansari, J. Řeháček, Z. Hradil, B. Stoklasa, M. Paúr, L. L. Sánchez-Soto, and C. Silberhorn, Physical Review Letters 121, 090501 (2018).
- [58] S. Ragy, M. Jarzyna, and R. Demkowicz-Dobrzański, Physical Review A 94, 052108 (2016).
- [59] A. Chrostowski, R. Demkowicz-Dobrzański, M. Jarzyna, and K. Banaszek, International Journal of Quantum Information 15, 1740005 (2017).
- [60] J. Yang, S. Pang, Y. Zhou, and A. N. Jordan, Physical Review A 100, 032104 (2019).
- [61] J. R. Hervas, L. L. Sánchez-Soto, A. Z. Goldberg, Z. Hradil, and J. Řeháček, Physical Review A 110, 033716 (2024).
- [62] S. Z. Ang, R. Nair, and M. Tsang, Physical Review A 95, 063847 (2017).
- [63] Z. Yu and S. Prasad, Physical Review Letters 121, 180504 (2018).
- [64] S. Prasad, Physica Scripta **95**, 054004 (2020).
- [65] B. Wang, L. Xu, J.-c. Li, and L. Zhang, Photonics Research 9, 1522 (2021).
- [66] C. Napoli, S. Piano, R. Leach, G. Adesso, and T. Tufarelli, Physical Review Letters 122, 140505 (2019), arxiv:1805.04116 [cond-mat, physics:physics, physics:quant-ph].
- [67] R. K. Gosalia, R. Malaney, R. Aguinaldo, and J. Green, Laser Physics 34, 025201 (2024).
- [68] S. Prasad, Physical Review A 102, 063719 (2020), arxiv:2008.09946 [quant-ph].
- [69] L. Mandel, Proceedings of the Physical Society 74, 233 (1959).
- [70] J. Yang, S. Pang, Y. Zhou, and A. N. Jordan, Physical Review A 100, 032104 (2019).
- [71] J. Liu, H. Yuan, X.-M. Lu, and X. Wang, Journal of Physics A: Mathematical and Theoretical 53, 023001 (2020).
- [72] J. Suzuki, Journal of Mathematical Physics 57, 042201 (2016).

Appendix A: Resolution limit of direct imaging

Suppose the probability distribution of a single photon arriving on the two-dimensional image plane is given by

$$p_{\mathbf{g}}(x,y) = \frac{1-\epsilon}{2}\Lambda(x - X_1, y - Y_1) + \frac{1+\epsilon}{2}\Lambda(x - X_2, y - Y_2),\tag{A1}$$

where $(X_{1,2}, Y_{1,2}) = (\bar{X} \mp \frac{r}{2}\cos\alpha, \bar{Y} \mp \frac{r}{2}\sin\alpha)$. The photon counting at a small area $dx \times dy$ around the position (x, y) of the detector is approximately $(N_1 + N_2)p_{\mathbf{g}}(x, y)dxdy$, and the intensity $\Lambda(x, y)$ is determined by the point-spread function of imaging system

$$\Lambda(x,y) = |\psi(x,y)|^2. \tag{A2}$$

Assuming the probability distribution is parametrized by $\hat{\mathbf{g}} = (\hat{g}_1, \dots, \hat{g}_n)^{\mathsf{T}}$, the covariance matrix of any unbiased estimator $\hat{\mathbf{g}} = (\hat{g}_1, \dots, \hat{g}_n)^{\mathsf{T}}$ is lower bounded by the Cramér-Rao inequality [21, 70, 71],

$$Cov[\hat{\mathbf{g}}] \ge N_{\text{tot}} \mathcal{J}^{-1}[\mathbf{g}],\tag{A3}$$

where $N_{\rm tot}$ is total number of photons from the two optical sources,

$$N_{\text{tot}} = N_1 + N_2. \tag{A4}$$

The " \geq " sign represents semi-definite positivity of matrix, and $\mathcal{J}[\mathbf{g}]$ is the Fisher information matrix per photon detection,

$$\mathcal{J}_{ij} = \int_{-\infty}^{\infty} dy \int_{-\infty}^{\infty} dx \frac{1}{p_{\mathbf{g}}(x,y)} \frac{\partial p_{\mathbf{g}}(x,y)}{\partial g_i} \frac{\partial p_{\mathbf{g}}(x,y)}{\partial g_j}.$$
 (A5)

When the total photon number $N_{\rm tot}$ is sufficiently large, the Cramér-Rao bound inequality can always be asymptotically achieved via the maximum likelihood estimation strategy (MLE) [21], i.e., $\lim_{N_{\rm tot}\to\infty} \text{Cov}[\hat{\mathbf{g}}] = N_{\rm tot} \mathcal{J}^{-1}[\mathbf{g}]$.

For the task of resolving two point sources, the positions of the two sources, (X_1, Y_1) and (X_2, Y_2) , or equivalently the centroid $(\bar{X}, \bar{Y}) = (\frac{X_2 + X_1}{2}, \frac{Y_2 + Y_1}{2})$, the distance r and the azimuth α are unknown, so the unknown parameter vector \mathbf{g} to estimate is $\mathbf{g} = (\bar{X}, \bar{Y}, r, \alpha)^{\top}$.

For the direct imaging with an ideal continuum photodetector on the image plane, when the distance r is small, one can expand the Fisher information matrix \mathcal{J} to the second order of r, and the diagonal elements are

$$\mathcal{J}_{11} = c_{1,0} - \frac{1}{8}r^2 \left\{ a_{2,2} \sin^2 \alpha + (2\epsilon^2 + 1) b_{2,0} \sin(2\alpha) + (2\epsilon^2 + 1) c_{2,0} \cos^2 \alpha + 2\epsilon^2 \left[\sin^2 \alpha \left(c_{1,1} - t_{1,1} \right) - \cos^2 \alpha f_{1,0} - q_{1,0} \sin(2\alpha) \right] \right\}, \\
\mathcal{J}_{22} = c_{0,1} - \frac{1}{8}r^2 \left[a_{2,2} \cos^2 \alpha + (2\epsilon^2 + 1) \sin \alpha \left(2b_{0,2} \cos \alpha + c_{0,2} \sin \alpha \right) + 2\epsilon^2 \left(\cos^2 \alpha \left(c_{1,1} - t_{1,1} \right) - q_{0,1} \sin(2\alpha) - f_{0,1} \sin^2 \alpha \right) \right], \tag{A6}$$

$$\mathcal{J}_{33} = \frac{1}{4}\epsilon^2 \left(a_{1,1} \sin(2\alpha) + c_{0,1} \sin^2 \alpha + c_{1,0} \cos^2 \alpha \right) + \frac{r^2}{64} \left[(2 - 5\epsilon^2) a_{2,2} \sin^2(2\alpha) + 8\epsilon^4 \sin(2\alpha) \left(q_{1,0} \cos^2 \alpha + q_{0,1} \sin^2 \alpha \right) + 4 \left(2 - 5\epsilon^2 \right) \sin(2\alpha) \left(b_{0,2} \sin^2 \alpha + b_{2,0} \cos^2 \alpha \right) + 2 \left(2 - 5\epsilon^2 \right) \left(c_{1,1} \sin^2(2\alpha) + c_{2,0} \cos^4 \alpha + c_{0,2} \sin^4 \alpha \right) + 4\epsilon^4 \left(f_{0,1} \sin^4 \alpha + f_{1,0} \cos^4 \alpha \right) + 6\epsilon^4 t_{1,1} \sin^2(2\alpha) \right],$$

$$\mathcal{J}_{44} = \frac{1}{4}r^2 \epsilon^2 \left(c_{1,0} \sin^2 \alpha + c_{0,1} \cos^2 \alpha - a_{1,1} \sin(2\alpha) \right),$$

and the off-diagonal elements of ${\mathcal J}$ are

$$\mathcal{J}_{12} = \mathcal{J}_{21} = a_{1,1} - \frac{1}{8}r^2 \left[\left(2\epsilon^2 + 1 \right) b_{2,0} \cos^2 \alpha + \left(2\epsilon^2 + 1 \right) b_{0,2} \sin^2 \alpha - 2\epsilon^2 \left(q_{0,1} \sin^2 \alpha + q_{1,0} \cos^2 \alpha \right) \right. \\ \left. + \epsilon^2 a_{2,2} \sin(2\alpha) + \left(\epsilon^2 + 1 \right) c_{1,1} \sin(2\alpha) - 2\epsilon^2 t_{1,1} \sin(2\alpha) \right],$$

$$\mathcal{J}_{13} = \mathcal{J}_{31} = \frac{\epsilon}{2} \left(c_{1,0} \cos \alpha + a_{1,1} \sin \alpha \right) - \frac{\epsilon r^2}{16} \left[\left(2\epsilon^2 + 1 \right) a_{2,2} \sin^2 \alpha \cos \alpha \right]$$

$$+ (2\epsilon^{2} + 1) b_{0,2} \sin^{3} \alpha + 3 (2\epsilon^{2} + 1) b_{2,0} \sin \alpha \cos^{2} \alpha$$

$$+ 2 (2\epsilon^{2} + 1) c_{1,1} \sin^{2} \alpha \cos \alpha + (2\epsilon^{2} + 1) c_{2,0} \cos^{3} \alpha$$

$$- 2\epsilon^{2} (f_{1,0} \cos^{3} \alpha + 3 \sin \alpha \cos^{2} \alpha q_{1,0} + q_{0,1} \sin^{3} \alpha + 3t_{1,1} \sin^{2} \alpha \cos \alpha) \right],$$

$$\mathcal{J}_{14} = \mathcal{J}_{41} = \frac{1}{2} r \epsilon (a_{1,1} \cos \alpha - c_{1,0} \sin \alpha),$$

$$\mathcal{J}_{23} = \mathcal{J}_{32} = \frac{1}{2} \epsilon (a_{1,1} \cos \alpha + c_{0,1} \sin \alpha) - \frac{r^{2} \epsilon}{16} \left[(2\epsilon^{2} + 1) a_{2,2} \sin \alpha \cos^{2} \alpha + (2\epsilon^{2} + 1) b_{2,0} \cos^{3} \alpha + 3 (2\epsilon^{2} + 1) b_{0,2} \sin^{2} \alpha \cos \alpha$$

$$+ (2\epsilon^{2} + 1) c_{0,2} \sin^{3} \alpha + 2 (2\epsilon^{2} + 1) c_{1,1} \sin \alpha \cos^{2} \alpha$$

$$- 2\epsilon^{2} f_{0,1} \sin^{3} \alpha - 2\epsilon^{2} q_{1,0} \cos^{3} \alpha - 6\epsilon^{2} q_{0,1} \sin^{2} \alpha \cos \alpha$$

$$- 6\epsilon^{2} t_{1,1} \sin \alpha \cos^{2} \alpha \right],$$

$$\mathcal{J}_{24} = \mathcal{J}_{42} = \frac{1}{2} r \epsilon (c_{0,1} \cos \alpha - a_{1,1} \sin \alpha),$$

$$\mathcal{J}_{34} = \mathcal{J}_{43} = \frac{1}{8} r \epsilon^{2} [2a_{1,1} \cos(2\alpha) + (c_{0,1} - c_{1,0}) \sin(2\alpha)],$$

$$(A7)$$

where

$$a_{i,j} = \int_{-\infty}^{\infty} dy \int_{-\infty}^{\infty} dx \frac{\Lambda^{(i,0)}(x,y)\Lambda^{(0,j)}(x,y)}{\Lambda(x,y)}, i, j = 1, 2,$$

$$b_{i,j} = \int_{-\infty}^{\infty} dy \int_{-\infty}^{\infty} dx \frac{\Lambda^{(i,j)}(x,y)\Lambda^{(1,1)}(x,y)}{\Lambda(x,y)}, i, j = 0, 1, 2,$$

$$c_{i,j} = \int_{-\infty}^{\infty} dy \int_{-\infty}^{\infty} dx \frac{\Lambda^{(i,j)}(x,y)^{2}}{\Lambda(x,y)}, i, j = 0, 1, 2,$$

$$f_{i,j} = \int_{-\infty}^{\infty} dy \int_{-\infty}^{\infty} dx \frac{\Lambda^{(i,j)}(x,y)^{4}}{\Lambda(x,y)^{3}}, i, j = 0, 1,$$

$$q_{i,j} = \int_{-\infty}^{\infty} dy \int_{-\infty}^{\infty} dx \frac{\Lambda^{(0,1)}(x,y)\Lambda^{(1,0)}(x,y)\Lambda^{(i,j)}(x,y)^{2}}{\Lambda(x,y)^{3}}, i, j = 0, 1,$$

$$t_{1,1} = \int_{-\infty}^{\infty} dy \int_{-\infty}^{\infty} dx \frac{\Lambda^{(0,1)}(x,y)\Lambda^{(1,0)}(x,y)\Lambda^{(i,j)}(x,y)^{2}}{\Lambda(x,y)^{3}}.$$
(A8)

Considering the variance of the distance r may diverge when $r \to 0$, we use the reciprocal of the variance to quantify the estimation precision of r, the result can be worked out as

$$\mathcal{H}_r^{\text{(direct)}} = N_{\text{tot}} / (\mathcal{J}^{-1})_{33} = \frac{r^2 \left(1 - \epsilon^2\right)^2 N_{\text{tot}}}{16} \mathcal{A},\tag{A9}$$

where

$$\mathcal{A} = 2a_{2,2}\sin^2\alpha\cos^2\alpha + 2\left(b_{2,0}\cos^2\alpha + b_{0,2}\sin^2\alpha\right)\sin 2\alpha + c_{0,2}\sin^4\alpha + c_{1,1}\sin^2 2\alpha + c_{2,0}\cos^4\alpha. \tag{A10}$$

As the precision $\mathcal{H}_r^{\text{(direct)}}$ drops quadratically as the distance r decreases, it vanishes when r approaches zero, implying no information about r can be obtained when the two point sources are too close to each other. This phenomenon is called Rayleigh's curse [20].

Appendix B: Precision of quantum superresolution

1. Multiparameter quantum estimation theory for superresolution

The quantum parameter estimation theory provides a mathematical tool to address Rayleigh's curse for two closely spaced optical point sources. In general, it takes into account the parameters in a quantum system and further

optimizes the estimation precision over all possible measurement bases in addition to the optimization of estimation strategies involved in the classical Cramér-Rao bound. The precision of quantum estimation is characterized by the quantum Cramér-Rao bound,

$$\operatorname{Cov}[\hat{\mathbf{g}}] \ge N_{\text{tot}}^{-1} \mathcal{Q}_{ij}^{-1}[\mathbf{g}],\tag{B1}$$

where Q is the quantum Fisher information matrix, defined as

$$Q_{ij}(\hat{\rho}) = \frac{1}{2} \text{Tr}[\hat{\rho}\{\hat{\mathcal{L}}_{g_i}, \hat{\mathcal{L}}_{g_j}\}], \, \forall g_i, g_j \in \mathbf{g},$$
(B2)

where $\{\cdot,\cdot\}$ denotes the anticommutator and $\hat{\mathcal{L}}_{g_i}$ is the symmetric logarithmic derivative (SLD) of the density operator $\hat{\rho}$ with respect to the parameter g_i ,

$$\frac{1}{2}(\hat{\mathcal{L}}_{g_i}\hat{\rho} + \hat{\rho}\hat{\mathcal{L}}_{g_i}) = \partial_{g_i}\hat{\rho}. \tag{B3}$$

By decomposing the density matrix $\hat{\rho}$ in its orthogonal eigenvectors as

$$\hat{\rho} = \sum_{k} \lambda_k |\lambda_k\rangle \langle \lambda_k|,\tag{B4}$$

a SLD $\hat{\mathcal{L}}_{q_i}$ can be expressed as

$$\hat{\mathcal{L}}_{g_i} = \sum_{\lambda_h + \lambda_h \neq 0} \frac{2\langle \lambda_k | \partial_{g_i} \hat{\rho} | \lambda_h \rangle}{\lambda_k + \lambda_h} |\lambda_k \rangle \langle \lambda_h|. \tag{B5}$$

Since the density matrix (1) of two point sources has rank 2, the quantum Fisher information matrix is more conveniently calculated within the support of $\hat{\rho}$,

$$Q_{ij}(\hat{\rho}) = \sum_{\lambda_k \neq 0} \frac{4\langle \lambda_k | \partial_{g_i} \hat{\rho} \partial_{g_j} \hat{\rho} | \lambda_k \rangle}{\lambda_k} + \sum_{\lambda_k, \lambda_h \neq 0} 2\left(\frac{1}{\lambda_k + \lambda_h} - \frac{1}{\lambda_k} - \frac{1}{\lambda_h}\right) \langle \lambda_h | \partial_{g_i} \hat{\rho} | \lambda_k \rangle \langle \lambda_k | \partial_{g_j} \hat{\rho} | \lambda_h \rangle. \tag{B6}$$

In fact, the quantum Cramér-Rao bound for multiparameter estimation is not always achievable due to the potential non-commutativity between the optimal measurements for different parameters. But if one is interested in the overall estimation precision of different parameters, a positive-semidefinite weight matrix W can be imposed on the unknown parameters generally and the matrix form of quantum Cramér-Rao's bound can be simplified to a scalar form,

$$Tr(WC) \ge N_{\text{tot}}^{-1} Tr(WQ^{-1}). \tag{B7}$$

By introducing the weight matrix W, we can assign different weights to different unknown parameters. Furthermore, the quantum Cramér-Rao bound for the above scalar form can be saturated if

$$\operatorname{Tr}(\hat{\rho}[\hat{\mathcal{L}}_{g_i}, \hat{\mathcal{L}}_{g_j}]) = \operatorname{Im}\operatorname{Tr}(\hat{\rho}\hat{\mathcal{L}}_{g_i}\hat{\mathcal{L}}_{g_j}) = 0,$$
(B8)

where $[\cdot,\cdot]$ denotes the commutator, by recognizing that the quantum Cramér-Rao bound is equivalent to the Holevo bound when this condition is satisfied and the latter is always achievable asymptotically with a sufficiently large number of states [58, 72]. Note that for our current quantum superresolution problem, the compatibility condition (B8) is always fulfilled due to the reality of point-spread function which makes the symmetric logarithmic derivatives $\hat{\mathcal{L}}_{g_i}$ and $\hat{\mathcal{L}}_{g_j}$ also real according to Eq. (B3). So the quantum Cramér-Rao bound provides an achievable precision limit for the estimation of the distance between two incoherent point sources allowed by quantum mechanics [39, 58].

2. Quantum estimation precision of source distance

Building upon the pioneering quantum superresolution framework for one-dimensional imaging systems developed by Tsang et al. [20], we extend the superresolution theory to two incoherent optical point sources with arbitrary intensities in two-dimensional imaging systems. The quantum state of a single detected photon can be described by the density operator

$$\hat{\rho} = \frac{1 - \epsilon}{2} e^{-iX_1 \hat{P}_x} e^{-iY_1 \hat{P}_y} |\psi\rangle \langle\psi| e^{iX_1 \hat{P}_x} e^{iY_1 \hat{P}_y} + \frac{1 + \epsilon}{2} e^{-iX_2 \hat{P}_x} e^{-iY_2 \hat{P}_y} |\psi\rangle \langle\psi| e^{iX_2 \hat{P}_x} e^{iY_2 \hat{P}_y},$$
(B9)

which depends on the parameters $\mathbf{g} = (\bar{X}, \bar{Y}, r, \alpha)^{\top}$.

The support of the density matrix $\hat{\rho}$ (B9) is spanned by two eigenstates associated with nonzero eigenvalues,

$$|\lambda_{1,2}\rangle = \frac{1}{\sqrt{\mathcal{Q}_{1,2}}} \times \{e^{-iY_1\hat{P}_y}e^{-iX_1\hat{P}_x}|\psi\rangle \mp \frac{\left(\sqrt{\epsilon^2 + \delta^2(1 - \epsilon^2)} \mp \epsilon\right)}{\delta(1 - \epsilon)}e^{-iX_2\hat{P}_x}e^{-iY_2\hat{P}_y}|\psi\rangle\},\tag{B10}$$

where $\mathcal{Q}_{1,2}$ are the normalization constants,

$$\mathcal{Q}_{1,2} = \left(1 - \delta^2\right) \left(1 + \frac{\delta^2 \left(1 - \delta^2\right) (1 - \epsilon)^2}{\left(\sqrt{\delta^2 + \epsilon^2 - \delta^2 \epsilon^2} \pm \delta^2 (1 - \epsilon) \pm \epsilon\right)^2}\right),\tag{B11}$$

and δ is the overlap between two point-spread functions

$$\delta \equiv \langle \psi_1 \mid \psi_2 \rangle = \int_{-\infty}^{\infty} dx \int_{-\infty}^{\infty} dy \psi_1^*(x, y) \psi_2(x, y) \neq 0.$$
 (B12)

The eigenvalues are

$$\lambda_{1,2} = \frac{1}{2} \left(1 \mp \sqrt{\epsilon^2 + \delta^2 \left(1 - \epsilon^2 \right)} \right). \tag{B13}$$

Since the two point-spread functions are real, the overlap can be simplified to

$$\delta = \langle e^{-ir\cos\alpha \hat{P}_x} e^{-ir\sin\alpha \hat{P}_y} \rangle = \langle \cos(r\hat{P}_r) \rangle. \tag{B14}$$

According to Eq. (B6), the quantum Fisher information matrix with respect to unknown parameters $\mathbf{g} = (\bar{X}, \bar{Y}, r, \alpha)^{\mathsf{T}}$ can be derived by plugging the eigenvalues (B13) and eigenstates (B10) of the density matrix $\hat{\rho}$ into Eq. (B6), and the elements of the quantum Fisher information matrix \mathcal{Q} turn out to be

$$Q_{11} = 4\kappa_{x} - 4\left(1 - \epsilon^{2}\right)\gamma_{x}^{2},$$

$$Q_{12} = Q_{21} = 4\eta - 4\left(1 - \epsilon^{2}\right)\gamma_{x}\gamma_{y},$$

$$Q_{13} = Q_{31} = 2\epsilon\left(\eta\sin\alpha + \cos\alpha\kappa_{x}\right),$$

$$Q_{14} = Q_{41} = 2r\epsilon\left(\eta\cos\alpha - \sin\alpha\kappa_{x}\right),$$

$$Q_{22} = 4\kappa_{y} - 4\left(1 - \epsilon^{2}\right)\gamma_{y}^{2},$$

$$Q_{23} = Q_{32} = 2\epsilon\left(\eta\cos\alpha + \sin\alpha\kappa_{y}\right),$$

$$Q_{24} = Q_{42} = 2r\epsilon\left(\cos\alpha\kappa_{y} - \eta\sin\alpha\right),$$

$$Q_{33} = \kappa_{r},$$

$$Q_{34} = Q_{43} = \frac{r}{2}\left(2\eta\cos(2\alpha) - \sin(2\alpha)\kappa_{x} + \sin(2\alpha)\kappa_{y}\right),$$

$$Q_{44} = r^{2}\kappa_{r^{\perp}},$$
(B15)

where

$$\kappa_{x} = \langle \hat{P}_{x}^{2} \rangle, \kappa_{y} = \langle \hat{P}_{y}^{2} \rangle, \eta = \langle \hat{P}_{x} \hat{P}_{y} \rangle,
\kappa_{r^{\perp}} = \langle \hat{P}_{r^{\perp}}^{2} \rangle = \kappa_{x} \sin^{2} \alpha + \kappa_{y} \cos^{2} \alpha - \eta \sin(2\alpha),
\kappa_{r} = \langle \hat{P}_{r}^{2} \rangle = \eta \sin(2\alpha) + \cos^{2} \alpha \kappa_{x} + \sin^{2} \alpha \kappa_{y},
\gamma_{x} = i \langle \hat{P}_{x} e^{-ir\cos\alpha \hat{P}_{x}} e^{-ir\sin\alpha \hat{P}_{y}} \rangle = \langle \hat{P}_{x} \sin(r\hat{P}_{r}) \rangle,
\gamma_{y} = i \langle \hat{P}_{y} e^{-ir\cos\alpha \hat{P}_{x}} e^{-ir\sin\alpha \hat{P}_{y}} \rangle = \langle \hat{P}_{y} \sin(r\hat{P}_{r}) \rangle.$$
(B16)

In the present quantum superresolution problem, the primary parameter of interest is the distance r. To focus on the estimation precision of r, we introduce a weight matrix

so that Tr(WC) is the variance of r which is bounded by $N_{\text{tot}}^{-1}\text{Tr}(WQ^{-1})$, where C is the covariance matrix of the parameters $\mathbf{g} = (\bar{X}, \bar{Y}, r, \alpha)^{\top}$. By inverting the quantum Fisher information matrix Q, the estimation precision of the distance r can be determined as

$$\mathcal{H}_r = N_{\text{tot}}/(\mathcal{Q}^{-1})_{33} = \frac{\mathcal{H}_r^{\text{(num)}}}{\mathcal{H}_r^{\text{(den)}}},\tag{B18}$$

where the numerator is

$$\mathcal{H}_r^{(\text{num})} = N_{\text{tot}} \left(1 - \epsilon^2 \right) \left(\kappa_x \kappa_y - \eta^2 \right) \times \left[\kappa_x \kappa_y - \eta^2 + 2\eta \gamma_x \gamma_y - \kappa_x \gamma_y^2 - \gamma_x^2 \kappa_y \right], \tag{B19}$$

and the denominator is

$$\mathcal{H}_{r}^{(\text{den})} = (\kappa_{x}\kappa_{y} - \eta^{2}) \kappa_{r^{\perp}}$$

$$+ \gamma_{x}^{2} \left[\epsilon^{2} (\eta \sin \alpha - \kappa_{y} \cos \alpha)^{2} - \kappa_{r^{\perp}} \kappa_{y} \right]$$

$$+ \gamma_{x}\gamma_{y} \left[\epsilon^{2} (\kappa_{x}\kappa_{y} - \eta^{2}) \sin(2\alpha) + 2\eta \kappa_{r^{\perp}} (1 - \epsilon^{2}) \right]$$

$$+ \gamma_{y}^{2} \left[\epsilon^{2} (\eta \cos \alpha - \kappa_{x} \sin \alpha)^{2} - \kappa_{r^{\perp}} \kappa_{x} \right].$$
(B20)

We focus on the estimation precision \mathcal{H}_r in the sub-Rayleigh regime, where the distance r is much smaller than the classical diffraction limit. To investigate the quantum limit of estimating the distance r in this regime, we consider the precision \mathcal{H}_r in the asymptotic case $r \to 0$, which is reduced to

$$\mathcal{H}_r|_{r\to 0} = \frac{N_{\text{tot}} \left(1 - \epsilon^2\right) \left(\kappa_x \kappa_y - \eta^2\right)}{\kappa_{r\perp}}.$$
 (B21)

This result demonstrates that, while direct imaging fails with vanishing precision in the sub-Rayleigh regime, the quantum strategy achieves non-zero precision, thus beating Rayleigh's curse.

For two Gaussian point-spread functions, the quantities in Eq. (B21) become

$$\kappa_x = \frac{1}{4\sigma_1^2 (1 - \beta^2)},$$

$$\kappa_y = \frac{1}{4\sigma_2^2 (1 - \beta^2)},$$

$$\eta = -\frac{\beta}{4\sigma_1\sigma_2 (1 - \beta^2)}.$$
(B22)

The estimation precision for the distance r in the limit $r \to 0$, can be simplified to

$$\mathcal{H}_r|_{r\to 0} = \frac{\left(1 - \epsilon^2\right) N_{\text{tot}}}{4\left(\beta \sigma_2 \sigma_1 \sin(2\alpha) + \sigma_2^2 \sin^2(\alpha) + \sigma_1^2 \cos^2(\alpha)\right)},\tag{B23}$$

which shows \mathcal{H}_r keeps nonzero when r is zero.

3. Coordinate invariance of \mathcal{H}_r

While the precision limit \mathcal{H}_r (B21) seems dependent on the azimuth α which can change with the coordinate system, \mathcal{H}_r should be invariant with any change of the coordinate system as it is an inherent property of the two point sources irrelevant to what coordinate system we choose.

To verify the coordinate-independence of the \mathcal{H}_r , we first note that the factor $\kappa_x \kappa_y - \eta^2$ in the numerator of \mathcal{H}_r (B21) is actually the determinant of the following matrix,

$$\Pi = \begin{bmatrix} \kappa_x & \eta \\ \eta & \kappa_y \end{bmatrix}, \tag{B24}$$

with $\kappa_x = \langle \hat{P}_x^2 \rangle$, $\kappa_y = \langle \hat{P}_y^2 \rangle$, $\eta = \langle \hat{P}_x \hat{P}_y \rangle$. Under a global rotation of the coordinate system by an angle θ , the momentum operators \hat{P}_x , \hat{P}_y are transformed as

$$\begin{bmatrix} \hat{P}'_x \\ \hat{P}'_y \end{bmatrix} = R(\theta) \begin{bmatrix} \hat{P}_x \\ \hat{P}_y \end{bmatrix}, \tag{B25}$$

where

$$R(\theta) = \begin{bmatrix} \cos\theta & -\sin\theta \\ \sin\theta & \cos\theta \end{bmatrix}. \tag{B26}$$

So the matrix Π becomes

$$\Pi' = \begin{bmatrix} \kappa_x' & \eta' \\ \eta' & \kappa_y' \end{bmatrix} = R(\theta)^{\mathsf{T}} \Pi R(\theta), \tag{B27}$$

in the rotated basis.

Since a similarity transformation preserves the determinant of a matrix, we have

$$\det(\Pi') = \det(\Pi),\tag{B28}$$

so the quantity $\kappa_x \kappa_y - \eta^2$ remains invariant with the rotation of the coordinate system.

For the denominator of the precision \mathcal{H}_r in Eq. (B21), we show that this is equal to the mean square of the momentum along the direction orthogonal to the displacement between the two point sources, i.e.,

$$\kappa_{r^{\perp}} = \langle \hat{P}_{r^{\perp}}^2 \rangle = \kappa_x \sin^2 \alpha + \kappa_y \cos^2 \alpha - \eta \sin 2\alpha, \tag{B29}$$

where

$$\hat{P}_{r^{\perp}} = \hat{P}_y \cos \alpha - \hat{P}_x \sin \alpha. \tag{B30}$$

As the displacement between the two point sources is physically inherent to the sources, irrelevant to the choice of coordinate system, the momentum operator $\hat{P}_{r^{\perp}}$ in the direction orthogonal to the displacement between the two sources is a physical observable independent of the coordinate system, therefore, the mean square of $\hat{P}_{r^{\perp}}$ is physically determined and remains invariant under any coordinate rotation.

So, we can see that both the numerator and denominator of the precision \mathcal{H}_r (B21) are coordinate-invariant quantities: the numerator is the determinant of the matrix Π composed of the mean of the products of two momentum operators, and the denominator is the mean square of the momentum along the direction orthogonal to the displacement between the two sources. Consequently, \mathcal{H}_r is independent of the choice of the coordinate system and depends solely on the intrinsic geometric relation between the point-spread functions of the two sources.